FINITE ELEMENT FORMULATION
OF VISCOUS SEA ICE MODEL

SATTI VIJAYA BHASKARA REDDY

NOTICE

AVIS

The quality of this microfiche is heavily dependent upon the quality of the original thesis submitted for microfilming. Every effort has been made to ensure the highest quality of reproduction possible.

If pages are missing, contact the university which granted the degree.

Some pages may have indistinct print especially if the original pages were typed with a poor typewriter ribbon or if the university sent us a poor photocopy.

Previously copyrighted materials (journal articles, published tests, etc.) are not filmed.

Reproduction in full or in part of this film is governed by the Canadian Copyright Act, R.S.C. 1970, c. C-30. Please read the authorization forms which accompany this thesis.

La qualité de cette microfiche dépend grandement de la qualité de la thèse soumise au microfilmage. Nous avons tout fait pour assurer une qualité supérieure de reproduction.

S'il manque des pages, veuillez communiquer avec l'université qui a conféré le grade.

La qualité d'impression de certaines pages peut laisser à désirer, surtout si les pages originales ont été dactylographiées à l'aide d'un ruban usé ou si l'université nous a fait parvenir une photocopie de mauvaise qualité.

Les documents qui font déjà l'objet d'un droit d'auteur (articles de revue, examens publiés, etc.) ne sont pas microfilmés.

La reproduction, même partielle, de ce microfilm est soumise à la Loi canadienne sur le droit d'auteur, SRC 1970, c. C-30. Veuillez prendre connaissance des formules d'autorisation qui accompagnent cette thèse.

**THIS DISSERTATION
HAS BEEN MICROFILMED
EXACTLY AS RECEIVED**

**LA THÈSE A ÉTÉ
MICROFILMÉE TELLE QUE
NOUS L'AVONS REÇUE**

FINITE ELEMENT FORMULATION

OF

VISCOUS SEA ICE MODEL

by

Satti Vijaya Bhaskara Reddy, B.E.   ©

A Thesis submitted in partial fulfillment

of the requirements for the degree of

Master of Engineering

Department of Engineering and Applied Science

Memorial University of Newfoundland

January 1977

St. John's   Newfoundland

ABSTRACT

The steady drift of sea ice in the Arctic Basin has been calculated by using the Finite Element Method, assuming that the ice is a viscous material. The Arctic Basin is discretized into 9 x 13 square elements of size 250 km by 250 km. The constitutive relations proposed by Glen (1970) have been used in the modeling. The momentum and continuity equations are solved for the ice velocity due to wind stress ocean current and ocean tilt. The drift has been calculated for four seasons in a span of two years by using proper viscosities in summer and winter. The vector addition of ice velocities due to wind, ocean current and tilt are plotted as combined velocities for all four seasons Summer 1, Winter 1, Summer 2 and Winter 2.

The results of the Finite Element Method of analysis are compared with that of the Fourier Transform Method (Hibler, 1976) and it is found that the results obtained by both methods agree with each other in the middle of the Basin. A comparison between slip and no slip boundary condition is also presented. Boundary elements are used and an iterative procedure is followed to incorporate the nonlinear boundary conditions.

A non-steady drift of pack ice in the Strait of Belle Isle, which moves back and forth due to tidal streams and currents have been calculated by the Finite Element Method formulation. It is observed that the pack ice velocities are harmonic as are the water velocities but with a time lag which depends upon viscosity parameters of ice.

Various velocity fields have been plotted and all patterns of calculated velocities are observed to be realistic.

ACKNOWLEDGEMENTS

TABLE OF CONTENTS

LIST OF FIGURES

LIST OF TABLES

LIST OF SYMBOLS USED

B	Empirical constant relating to air-ice Ekman layer.
D	Empirical constant relating to water-ice Ekman layer.
F	Force due to variations in internal ice stress.
f	Coriolis parameter.
$\underline{G}$	Long term geostrophic currents.
g	Gravitational acceleration.
H	Sea surface height.
[K]	Matrix derived from the energy dissipation in ice-water system.
$\underline{k}$	Unit vector perpendicular to x-y plane.
L_1, L_2, L_3	Natural co-ordinates for a triangular element.
l_{ij}	Length parameter.
ℓ	Wave length of forcing function.
[M]	Mass matrix.
m	Mass of pack ice per unit area.
P	Atmospheric pressure.
{Q}	Load vector.
{q}	Generalised velocity vector.
S	Boundary line.
s	Variable length along boundary.
$\underline{T}$	Ocean tilt.
U	Velocity component in x direction.
V	Velocity component in y direction.
$\underline{u}$	Ice velocity vector.

τ_w Water stress on ice.

τ_a Air stress on ice.

θ Ekman angle in water.

ϕ Ekman angle in air.

ρ Density of air.

σ_{ij} Internal stress components in ice.

$\dot{\epsilon}_{ij}$ Strain-rate components.

$\dot{\gamma}_{xy}$ Strain-rate due to shear.

Ω Rotation of earth in radians per second.

λ Latitude.

ζ Bulk viscosity.

η Shear viscosity.

ω Frequency.

CHAPTER 1

INTRODUCTION

The factors affecting sea ice formation are salinity of water, wind, currents and the intensity of cooling. There are different types of ice in sea water. Fresh needle-like crystals closing together form a uniform sheet called young ice. The other types are pancake ice, fast ice on shores and pack ice. The Arctic pack ice covers large areas of the Arctic Ocean. The thickness of ice varies from zero to few meters. The pack ice sheets are observed in hundreds of meters across, and with patches of leads. Leads are open water or thin sheets of ice in the Arctic region. Pack ice is found during the greater part of the year in most portions of the marginal seas, Baffin Bay and the western part of the Labrador Sea, the Canadian Archipelago, Davis Strait and the East Greenland Coast.

Pack ice moves on the surface of sea water due to wind, ocean currents, body forces and interaction of neighboring ice. As it moves, it may heap up, lead ice into pressure ridges and hummocks in the form of rubble. The drift of ice is not generally noticeable to a person standing on it even though he might have moved hundreds of kilometers in a few months.

The drift of ice in the Arctic Basin has been discussed by Nansen (1902) and Sverdrup (1928), and it has been an important research field in recent years due to the recent discovery of hydrocarbon deposits in the Beaufort Sea. Antarctic ice drift was studied by Brennecke (1921) and the deviation angle between drift of ice and wind direction was found to be $34°$ to the left. The Nansen and Sverdrup studies of the deviation angle between the wind direction and the Arctic ice drift direction is $30°$ to the right. Nansen explained this deviation was due to the Coriolis force.

On the suggestion of Nansen, Ekman (1905) found that the effect of wind would be up to some depth in sea water. He observed that the velocities of different layers would deviate more and more as we go deeper and deeper in the water, but the magnitudes of velocity of different layers reduce exponentially with depth.

There are permanent drift tracks in the Arctic Basin which have been observed in recent years more closely than ever before (Figure 1.1). There is sufficient data available to acquire a rather accurate picture of the long term mean drift. The important drift tracks of ice in the Arctic Basin are a gyre in the Beaufort Sea and a transpolar drift stream. The drift pattern is very much wind driven. The small divergence and the difference in the import and export of ice have little effect on the gyre and the transpolar drift stream in the interior of the Basin.

Many scientists have proposed different models to predict the pack ice drift in the Arctic Basin. The idea behind mathematical modeling is to find out whether some realistic flow fields could be calculated, and more importantly, to see whether the pressure field within the ice cover can be interpreted sensibly in the light of known ice conditions in different areas of the basin.

There are two aspects of sea ice modeling which are not well understood, and different theories on ice drift have been proposed due to limited knowledge and data. The first aspect deals with the mechanical properties of ice in small scale, and the second aspect deals with the behavior of pack ice on a large scale. Considerable literature exists on the research in these two fields.

Ice is a crystalline material with hexagonal symmetry. Its characteristics, such as thickness, quality, and type of grain structure, are subject to variability with weather. Elasticity, plasticity and all mechanical properties are sensitive to temperature. Brine volume in sea ice has a noticeable influence on its properties. Statistics and probability theory are entering all fields of engineering, and their use in ice studies is indispensable. Several years of observation are necessary to establish useful information regarding ice properties on a small or large scale.

In view of the above mentioned factors, sea ice has been modeled as a viscous material by many scientists (Campbell,

1965, Glen,1970, Hibler,1974), as a plastic material by Coon (1972), as an elastic-plastic material by Coon, et al (1974) and as an inviscid fluid by Rothrock (1973).

A finite element formulation of the viscous sea ice model is presented here. Glen (1970) proposed the constitutive relations, and Hibler and Tucker (1976) proposed that the viscosity parameters in the viscous sea ice model vary according to the seasons. In the finite element analysis, a set of two linear differential equations with variable viscosity parameters are solved to obtain velocities of pack ice which is driven by wind, ocean current and ocean tilt. The results obtained by the finite element method are in good agreement with those obtained by other methods. The advantage of the finite element method is that it is capable of solving the differential equations over an irregular domain. Realistic boundary conditions can be incorporated by introducing the boundary elements whose properties change according to the conditions whether ice is pushing into or pulling away from the boundary. The results of computations are presented for the steady state ice drift in the Arctic Basin and the transient ice velocity of pack ice in the strait of Belle Isle which is driven by strong tidal streams.

CHAPTER 2

MECHANICAL BEHAVIOR OF PACK ICE

2.1 KINEMATICS

The velocity field of pack ice varies in space and in time. But velocities alone are poor indicators of ice behavior because the mechanical behavior of pack ice is related to velocity differences between floes, or the velocity gradients, that is vorticity and strain rate. Velocity gradients may be well defined in a continuum, but in a real ice cover they are not. Abrupt changes may take place at floe boundaries. To measure the response of ice to real weather systems, which may vary over a periods of about a day, the measurements should be arranged over periods of less than a day. Temporal averages are of not much use. If spacial averages are to be useful, there must be a continuum length of scale l_c which is large compared to floe size l_i and small compared to the smallest space scale l_f of the driving forces (Maykut, Thorndike and Untersteiner, 1972), that is, l_c is to exist such that

$$l_i < l_c < l_f \qquad (2.1)$$

The lengths l_i and l_f are not well defined, but in the Arctic Ocean rigid pieces of ice larger than 50 km across are rare, and atmospheric pressure systems in the Arctic Ocean

are typically 1000 km to 2000 km across.

Nye (1973a) proposed to smooth the velocity field eliminating variations shorter than l_c and then defining strain rates. But this idea is not practical. To obtain correct size of gauge length l_g, two methods have been adopted. In the first method, strain rates were simultaneously measured on a gauge of 100 km and on a gauge of 20 km and less. If both these gauge lengths are within the continuum scales, the measured strain rates would correlate perfectly. These measurements showed that the net dilatation over a 25 day period (Hibler, et al, 1974) was strongly dependent on the gauge length. It was clear that one did not obtain the same estimate of strain rate by measuring over these different gauge lengths. In the second method, Nye and Thomas (1974) showed that the variance of strain rate measurements decreases as the gauge length l_g increases, and this effect was observed upto a gauge length of 100 km. From these two methods, it appears that the continuum length scale is 100 km or larger.

From different data (Colony and Rash, 1975, Dunbar and Wittman, 1963), we now have a good idea of typical velocities, vorticities and strain rates in the central Arctic Ocean. Pack ice moves at speeds of 10 km/day, occasionally reaching twice that speed. The actual path followed by a point in the ice is several times the net distance it travels over a period of months.

Instantaneous strain rates can be as large as several

percent per day, but the long term averages are considerably smaller. During the 40 day period documented by Thorndike (1974), the mean rates of divergence and shear (defined as the sum and difference of principal strain rates) were 0.001 and 0.002 per day, respectively. These numbers reflect the tendency of ice to deform more in shear than in divergence or convergence. The vorticity (defined as the vertical component of curl $\underline{u}$, where $\underline{u}$ is the velocity), behaves much the same as the rate of shear.

From most of these observations, one can infer that there is much difference between 'intra' and 'interfloe' strain, and that the strain which contributes to the large scale circulation of pack ice is caused by the relative movement of pieces of ice and not by the continuous deformation of pieces themselves.

2.2 THE STATE VARIABLES OF ICE COVER

The study of the properties of pack ice is complicated as it depends on changes in weather. The ice thickness may increase due to ridging or rafting, or thermodynamic changes in weather. Some open leads may form due to ridging and rafting. Thus the continuously varying characteristics such as compactness and thickness of ice must be considered in the model of sea ice. There are different approaches followed by different scientists to include these effects in their models.

In one approach, the compactness C has been defined as the fraction of the area covered by ice. The remaining fraction (1-C) is covered by open water. Drogaitsev (1956) and Nikiforov (1957) assumed that the ice covered area C within the total area B is conserved ($\frac{dC}{dt} = 0$). This means that only the area covered by open water (B-C) can change. Doronin (1970) modified the above equation by introducing a source term in the compactness equation to allow for thermodynamic changes in C. In the case of ridging, one can include a sink term in the compactness equation.

A different but more complete approach is to introduce terms of ice thickness distribution, g(h), which is defined as the fraction of the area covered by ice in the thickness band h_1 to h_2 and is given by $\int_{h_1}^{h_2} g(h)\,dh$ (Maykut and Thorndyke, 1973).

AIDJEX scientists (Coon,et al.,1974) used a function Ψ as a redistribution function in the thickness distribution. This function describes the creation of open water and the transfer of ice from one thickness to another by rafting and ridging. They incorporated the above concept in the elastic-plastic model for sea ice.

In the viscous sea ice model, pack ice is treated as a viscous material which resists changes in area of ice cover by the bulk viscosity modulus and the shear deformation by shear viscosity modulus. These viscosity parameters vary according to the season.

2.3 MOMENTUM EQUATION

The model of pack ice will have a momentum equation for the steady state condition in the following form:

$$-mf \underline{k} \times \underline{u} + \underline{\tau}_w + \underline{\tau}_a + \underline{F} + \underline{G} + \underline{T} = 0 \qquad (2.2)$$

where $\underline{u}$ is the ice velocity whose components are u and v in the x and y directions, f the Coriolis parameter which is equal to twice the product of earth's rate of rotation and sine of latitude, $\underline{k}$ a unit vector normal to x-y plane, m the ice mass per unit area, $\underline{F}$ the force due to variations in the internal ice stress ($F_i = \sigma_{ij,j}$), $\underline{\tau}_w$ and $\underline{\tau}_a$ the water and air stresses on the ice, and $\underline{G}$ and $\underline{T}$ the effect of long term geostrophic currents and ocean tilt on the ice motion. The components of current and air stresses are given by a modified Ekman layer theory (Rothrock, 1975).

$$\tau_{a_x} = B \left(\cos\phi \ U_g - \sin\phi \ V_g \right)$$

$$\tau_{a_y} = B \left(\sin\phi \ U_g + \cos\phi \ V_g \right)$$

$$G_x + \tau_{w_x} = D \left\{ -\cos\theta \ (u - U_w) + \sin\theta \ (v - V_w) \right\} \qquad (2.3)$$

$$G_y + \tau_{w_y} = -D \left\{ \sin\theta \ (u - U_w) + \cos\theta \ (v - V_w) \right\}$$

where ϕ and θ are Ekman angles in the air and water, respectively, U_g and V_g are the x and y components of the geostrophic wind, and U_w and V_w are the x and y components of the geostrophic ocean flow beneath the Ekman layer. In equation

(2.3), the $\underline{G}$ components are those components linear in U_w and V_w. In the case when $\underline{G}$ is neglected, the sea ice is effectively considered to be moving across a stagnant ocean. The geostrophic current flow is computed from ocean height H as follows:

$$\underline{U}_w = g \; f^{-1} \; \underline{k} \times \underline{\nabla} H \qquad (2.4)$$

where g is the gravitational acceleration. The tilt component is given by

$$\underline{T} = -m \; g \; \underline{\nabla} H \qquad (2.5)$$

The geostrophic wind is related to the surface atmospheric pressure P by the following expression:

$$\underline{U}_g = (\rho_a \; f)^{-1} \; \underline{k} \times \underline{\nabla} P \qquad (2.6)$$

where ρ_a is the density of air.

As the earth rotates about its axis (7.29×10^{-5} radians/sec), a velocity vector on it is continuously changing relative to space. This change in velocity per second is the Coriolis acceleration and it is perpendicular to both the velocity vector and rotation vector of the earth. As pack ice has considerable mass, we cannot neglect the Coriolis force which is given by the first term in the momentum equation (2.2).

For the steady state condition, we have neglected the acceleration term on the right hand side of equation (2.2). This

was discussed by Buynitskiy (1951). Rothrock (1970) showed that the acceleration of pack ice is of the order of 10^{-5} cm/sec^2 as a typical value in the Arctic Basin on the time scale of one day. But when two floes collide, the time scale is very much shorter than one day and these small scale accelerations are almost certainly significant, in which case we have to include an $m\dot{u}$ term on the right hand side of equation (2.2).

The deformation behavior of pack can be treated as that of a highly damped material. The wind drags the ice over a relatively stationary ocean, opposed mostly by water drag and resistance of the ice cover to deformation. The wind usually changes so slowly that the ice offers little inertial resistance to it. The work of the wind is dissipated partly by work against internal stress and partly by work on the ocean. The kinetic energy of the ice cover and its changes are relatively unimportant in the Arctic Basin.

2.4 CONSTITUTIVE RELATIONS

In order to integrate the momentum equation (2.2), we need constitutive relations which relate the stress tensor to other variables in the problem. In understanding ice dynamics, this has been the greatest single stumbling block. Different scientists have used different constitutive relations treating pack ice as a viscous material (Campbell, 1965), an incompressible and inviscid fluid (Rothrock, 1973), a cavitating fluid (Niki-forov, et al, 1967, Doronin, 1970), and an elastic–plastic material (Coon, et al, 1974).

Glen (1970) discussed various constitutive relations for a viscous model and proposed a constitutive relation stating that the internal ice stress $\underline{F}$ is related to stress and strain rates in the ice. The following are the relations proposed by Glen:

$$\sigma_{ij} = 2 \eta \dot{\varepsilon}_{ij} + (\zeta - \eta) \dot{\varepsilon}_{kk} \delta_{ij} \qquad (2.7)$$

$$F_i = \sigma_{ij,j} = \eta \nabla^2 u_i + \zeta \nabla_i (\nabla_k u_k) \qquad (2.8)$$

where η and ζ are shear and bulk viscosities characterising the ice cover on the geophysical scale, and $\dot{\varepsilon}_{ij}$ are the strain rate components given below

$$\dot{\varepsilon}_{ij} = \tfrac{1}{2}(u_{i,j} + u_{j,i}) \qquad (2.9)$$

Substituting equations (2.7 to 2.9) into

equation (2.2), a system of two coupled second order
linear partial differential equations is obtained for the
drift rate u(x,y) and v(x,y).

Hibler and Tucker (1976) estimated the values of bulk
and shear viscosities by correlating the observed and predicted
drift rates, and they found that the viscosity values giving
the best fit between the observed and predicted values show
a pronounced seasonal variation that correlates well with ice
growth rate. They suggested the following empirical linear
relationship between viscosity and ice growth rate which
yields predictions in reasonable agreement with both long
(yearly) and short (monthly) term observed drift rates:

$$\ln(\eta) = \ln(\zeta) = 0.92 \langle G \rangle + 24.73 \qquad (2.10)$$

where $\langle G \rangle$ is the 60 day averaged growth rate which varies
according to season. The range of best fit values of
viscosity is from 10^{10} to 4×10^{11} kg/sec.

CHAPTER 3

FINITE ELEMENT METHOD FORMULATION

3.1 INTRODUCTION

The Finite Element Method is one of the popular numerical techniques which is finding a place in a wide variety of engineering problems. The approximate solution is obtained at a few selected points (nodes) of a domain.

In a continuum problem of any dimension the field variable (whether it is pressure, temperature, velocity, stress or some other quantity) possesses an infinite number of values because it is a function of each generic point in the body or solution region. Consequently the problem is one with an infinite number of unknowns. In the finite element method, the solution region is discretized into elements. Element boundaries are connected with specified points called nodes or nodal points. Now we express the unknown field variable in terms of assumed approximate functions called interpolation functions within each element. These interpolation functions are defined in terms of the values of the field variables at the nodal points. Thus, the problem is reduced to one of a finite number of unknowns of the field variable at the nodal points. The

individual element properties can be formulated by one of the
following four approaches:- the direct approach, the variatio-
nal approach, the weighted residuals approach and the energy
balance approach. The choice of these approaches depends on
the type of the problem.

In the present problem, we use the variational approach.
In the classical variational formulation, the problem is to
find the unknown function or functions, which make stationary
a functional or functionals, subjected to some given boundary
conditions.

One of the important
advantages of the variational approach is that it implicitly
imposes the natural boundary conditions. In the finite ele-
ment method, we explicitly impose geometric boundary condi-
tions. Thus, in this method both types of boundary conditions
are satisfied. The finite element method can be applied to pro-
blems with complicated boundary conditions and irregular
shaped boundaries.

3.2 THE FINITE ELEMENT FORMULATION

The momentum equation is written with the inertial term in the following form:

$$-m \ f \ \underline{k} \times \underline{u} + \underline{\tau}_w + \underline{\tau}_a + \underline{F} + \underline{G} + \underline{T} - m \ \underline{\dot{u}} = 0 \qquad (2.2a)$$

where 'mu' is the change of momentum per unit area. In solving the momentum equation, we take ice velocity components as unknowns. A compatible velocity field is assumed in order to have a continuum which does not overlap or has holes in it during deformation. Strain rates are obtained by spacial differentiation of velocity components. Stress components can be obtained in terms of strain rate components by the use of constitutive relations. Thus, the set of two equations (2.2a) can be expressed in terms of velocity components u and v.

For the finite element formulation, we need a functional as explained in section (3.1), and this is obtained by multiplying the momentum equations (2.2a) by variations of u and v and integrating the sum of products over the domain. Thus, we have

$$\delta \Pi = \iint_{C} \begin{bmatrix} \delta u & \delta v \end{bmatrix} \begin{bmatrix} 0 & 2m\Omega\sin\lambda \\ \\ -2m\Omega\sin\lambda & 0 \end{bmatrix} \begin{bmatrix} u \\ v \end{bmatrix}$$

$$+ \begin{bmatrix} -D\cos\theta & D\sin\theta \\ -D\sin\theta & -D\cos\theta \end{bmatrix} \begin{bmatrix} u-U_w \\ v-V_w \end{bmatrix} + \begin{bmatrix} B\cos\phi & -B\sin\phi \\ B\sin\phi & B\cos\phi \end{bmatrix} \begin{bmatrix} U_g \\ V_g \end{bmatrix}$$

$$+ \begin{bmatrix} \sigma_{xx,x} + \tau_{xy,y} + T_x \\ \tau_{xy,x} + \sigma_{yy,y} + T_y \end{bmatrix} - \begin{bmatrix} m & 0 \\ 0 & m \end{bmatrix} \begin{bmatrix} \dot{u} \\ \dot{v} \end{bmatrix} \Bigg) \; dA = 0 \qquad (3.1)$$

where Ω is the earth's rate of rotation, λ is the latitude, and σ_{ij} is the two dimensional stress tensor whose components are the vertically integrated quantities across the thickness of pack ice. The units of σ_{ij} are force per unit length.

Integrating some of the terms in the above equation (3.1) by parts, we can express the functional in the following form by using the constitutive relations (2.7) and the equation (2.9):

$$\Pi = \iint \Bigg\{ \frac{1}{2} \begin{bmatrix} u & v \end{bmatrix} \begin{bmatrix} -D\cos\theta & D\sin\theta \\ & +2m\Omega\sin\lambda \\ -D\sin\theta & -D\cos\theta \\ -2m\Omega\sin\lambda & \end{bmatrix} \begin{bmatrix} u \\ v \end{bmatrix}$$

$$+ \begin{bmatrix} u & v \end{bmatrix} \begin{bmatrix} D\cos\theta & -D\sin\theta \\ D\sin\theta & D\cos\theta \end{bmatrix} \begin{bmatrix} U_w \\ V_w \end{bmatrix}$$

$$+ \begin{bmatrix} u & v \end{bmatrix} \begin{bmatrix} B\cos\phi & -B\sin\phi \\ B\sin\phi & B\cos\phi \end{bmatrix} \begin{bmatrix} U_g \\ V_g \end{bmatrix}$$

$$+ \begin{bmatrix} u & v \end{bmatrix} \begin{bmatrix} \tau_x \\ \tau_y \end{bmatrix}$$

$$- \frac{1}{2} \begin{bmatrix} u_{,x} & v_{,y} & u_{,y}+v_{,x} \end{bmatrix} \begin{bmatrix} \zeta+\eta & \zeta-\eta & 0 \\ \zeta-\eta & \zeta+\eta & 0 \\ 0 & 0 & \eta \end{bmatrix} \begin{bmatrix} u_{,x} \\ v_{,y} \\ u_{,y}+v_{,x} \end{bmatrix}$$

$$- \begin{bmatrix} u & v \end{bmatrix} \begin{bmatrix} m & 0 \\ 0 & m \end{bmatrix} \begin{bmatrix} \dot{u} \\ \dot{v} \end{bmatrix} \Bigg\} \, dA + \int_{S_f} \begin{bmatrix} u_n & u_t \end{bmatrix} \begin{bmatrix} \sigma_{nn} \\ \tau_{nt} \end{bmatrix} ds \tag{3.2}$$

where u_n, u_t, σ_{nn} and τ_{nt} are the velocity and stress components relative to the coordinate system $\underline{n}$ and $\underline{t}$ which are the unit outward normal and unit tangent vectors at the boundary, S_f is that part of the boundary where boundary forces are prescribed (see Figure A-2).

In the above functional (3.2), we note that there are some terms which represent the rate of work done by external forces, and there are other terms which represent the rate of energy dissipation. When the functional is stationary (i.e, $\delta \Pi = 0$),

the incremental rate of work done by external forces is equal
to the incremental rate of energy dissipation which takes
place in the form of deformation of pack ice, drag due to
water and the change of kinetic energy.

For the finite element formulation, the functional (3.2)
over the whole domain can be written as the sum of the functional
over finite size elements into which the whole domain is
discretized. Thus, we have

$$\Pi = \Sigma \ \Pi_e$$

where Π_e represents the functional (3.2) in which the integra-
tion is performed over element area and boundary.

A bilinear interpolation function is assumed for each
of the velocity components in a triangular element. The
derivation of element matrices, defining the element proper-
ties, is given in the Appendix A. These element matrices
are derived from the functional (3.2). After assembling the
element matrices, we can represent the first variation of
functional (3.2) in the following form:

$$\delta\Pi = \delta\{q\}^t \left[-[K]\{q\} - [M]\{\dot{q}\} + \{Q\} \right] = 0 \qquad (3.3)$$

where [K] is the matrix derived from the energy dissipation
due to water drag and deformation of pack ice, [M] the mass
matrix derived from the kinetic energy expression, {Q} the

generalised force vector representing the forces caused by
wind, currents and ocean tilt, and {q} the generalised nodal
velocity vector of the system.

If δ{q} is to be arbitrary, equation (3.3) requires that

$$[M]\{\ddot{q}\} + [K]\{q\} = \{Q\} \qquad (3.4)$$

The above equations are solved to obtain the nodal
velocities of the system. For computations of pack ice
drift in the Arctic Basin, only the steady state velocities
are calculated due to the small contribution of the inertial term
in relation to the other terms in the momentum equation (2.2).
Hence, we solve the following equation for steady state pack
ice drift.

$$[K]\{q\} = \{Q\} \qquad (3.5)$$

The finite element program, written by Desai and Abel
(1972), was modified to compute velocity of pack ice using
the formulation given above. In this program, four triangular
elements are assembled to make a general quadrilateral element
by eliminating the internal node by the static condensation
process (Desai and Abel, 1972). The resulting algebraic sys-
tem of equations after assembling the element properties give
rise to an unsymmetric banded matrix. A new subroutine was
written to solve a system of algebraic equations with

unsymmetric banded matrix by the method of decomposition of
the matrix into lower and upper triangular matrices. Several
other steps were incorporated in the program in order to com-
pute consistent generalised forces at the nodes which are des-
cribed in Appendix A.

Runge-Kutta mehtod of integration of the first order
equation (3.4) is also incorporated in the program in order
to compute time dependent velocity of pack ice. For the first
order system in time, there is a characteristic time for the
system which is an indicator of the response time of the
system, and it depends upon the inertial mass and the energy
dissipating property of the system. When the viscosity para-
meters are large, as they are for the pack ice in the Arotic
Basin, the response time is small, and we may as well solve
the steady state velocity of pack ice using equation (3.5).
For the loosely compacted ice, the viscosity parameters may
be small, and we may integrate the equation (3.4) using a time
step equal to a fraction of the characteristic time of the
system.

CHAPTER 4

RESULTS OF COMPUTATION

4.1 INTRODUCTION

In this chapter, we present the results of finite element analysis of the ice drift in the Arctic Ocean and in the Strait of Belle Isle using viscous sea ice model described in previous chapters.

In order to check the finite element computer program, some hypothetical atmospheric pressure variations are assumed and the resulting wind stress (equations 2.3 and 2.6) is imposed on the pack ice. The results obtained by finite element method were compared with the results obtained by Fourier Transform method. The agreement was found to be excellent. The program was then used to compute velocity of pack ice due to forces caused by wind, currents and ocean tilt. The velocities of pack ice obtained from each forcing function were superposed to obtain the overall ice velocity. We present the results of our calculations for a two year period using different values or viscosities in summer and winter.

The finite element method allows one to prescribe any kind of kinematic or force type boundary condition on any irregular boundary. But the boundary conditions are different

in the cases when the ice cover is pushed against the shore
and when it is receding from the shore. A special boundary
element is incorporated and an iterative scheme is followed
to take care of this special boundary condition.

Finally, we present the results of some of our cal-
culations on the motion of ice in the Strait of Belle Isle
which is driven back and forth by strong tidal streams and
currents.

4.2 HYPOTHETICAL ATMOSPHERIC PRESSURE VARIATIONS

In order to check the finite element computer program, we calculate the pack ice velocities due to wind stresses only, and we compare the results with the exact solution for a particular case when the atmospheric pressure variation is given by the following function.

$$P(x,y) = P_o \sin \frac{\pi x}{\ell} \sin \frac{\pi y}{\ell} \qquad (4.1)$$

where $\quad \ell = 2000$ km $\quad$ and $\quad P_o = 1000$ Pa(N/m^2)

This pressure variation creates a clockwise wind velocity field around the centre of 2000 km by 2000 km square area as shown in Figure 4.1. The geostrophic wind velocity components are obtained by using equation (2.6) as follows

$$U_g = -\frac{1}{\rho \ell} \frac{\partial P}{\partial y} = -\frac{\pi}{\ell} \frac{P_o}{\rho \ell} \sin \frac{\pi x}{\ell} \cos \frac{\pi y}{\ell}$$

$$\qquad (4.2)$$

$$V_g = \frac{1}{\rho \ell} \frac{\partial P}{\partial x} = \frac{\pi}{\ell} \frac{P_o}{\rho \ell} \cos \frac{\pi x}{\ell} \sin \frac{\pi y}{\ell}$$

where ρ (density of air) = 1.3 kg m^{-3} and f (Coriolis parameter) = 1.46 × 10^{-4} s^{-1}.

The components of air and water stresses are obtained from equations (2.3) using the following values of different parameters:

$$B = 0.01462 \text{ kg s}^{-1} \text{ m}^{-2}$$
$$D = 0.59 \text{ kg s}^{-1} \text{ m}^{-2}$$
$$\phi = \theta = 30^\circ$$

The mass of pack ice per unit area is calculated from the average thickness of ice in the Arctic Basin:

$$m = 3.0 \times 10^3 \text{ kg m}^{-2}$$

The exact solution of pack ice drift over a stagnant ocean due to the atmospheric pressure variations given in equation (4.1) is available using the Fourier Transform method in which the solution is repeated every 4000 km over an infinite domain in the x and y directions.

For the finite element analysis, the 2000 km by 2000 km square area is discretized into 8x8=64 square elements of size 250 km by 250 km. While using finite element method for this case, the values of ice velocity obtained from the exact solution are prescribed only at the boundary of a 2000 km by 2000 km square area to generate a solution inside the area.

The results of the finite element analysis are compared with the exact solution using two sets of values of shear and bulk viscosities:

$$\eta = \zeta = 2 \times 10^{10} \text{ kg s}^{-1}$$
$$\eta = \zeta = 4 \times 10^{11} \text{ kg s}^{-1}$$

In both cases, an excellent agreement is obtained between the exact solution and the results of finite element analysis. The velocity fields of pack ice are presented in Figure 4.2a and Figure 4.2b.

One can observe from Figures 4.2a and b that there is convergence when low values of viscosity are used, and divergence of pack ice occurs due to high values of viscosity. This is due to the Coriolis force which makes the pack ice converge for low values of viscosity. For high values of viscosity, pack ice offers greater resistance to Coriolis force, and it diverges under the influence of wind stresses. Dependence of convergence or divergence upon the values of shear and bulk viscosities was first pointed out by Hibler (1974).

This check on the results of finite element analysis confirms the correct implementation of finite element program.

4.3 PACK ICE DRIFT IN ARCTIC OCEAN

The external forces which make the pack ice move are mainly caused by the geostrophic wind, geostrophic current and ocean tilt. The Coriolis force and the drag force also influence the movement of pack ice and these forces are dependent upon the ice velocity. Since the system of differential equations governing the motion of pack ice are linear, we can solve for the ice velocities due to each forcing function separately and add the ice velocity components obtained from different types of forces to obtain the combined velocity of pack ice.

The Arctic Basin is discretized into 9x13 = 117 square elements of size 250 km by 250 km as shown in Figure 4.3. For the boundary conditions, the velocity of ice normal to boundary and the tangential shear stresses at the boundary are prescribed to be equal to zero. This means that the ice is allowed to slip at the boundary without any frictional resistance from the shore. The values of parameters used in the computations are same as those in the previous section except for the values of shear and bulk viscosities which are taken equal to 4×10^{10} kg s^{-1} for summer season and 3×10^{11} kg s^{-1} for winter season.

The wind stress acting on the pack ice can be computed from the atmospheric pressure data using equations (2.3) and (2.6). Four sets of atmospheric pressure data for the Arctic Basin were obtained from the Cold Regions Research and Engineering Laboratory, Hanover, N.H., (Hibler,1976). Each set of data is 180 day averaged atmospheric pressure at points on

a 250 km by 250 km grid system in the Arctic Basin. Thus, the computations were performed using atmospheric pressure data, given in Tables 4.1 to 4.4, for four seasons Summer 1, Winter 1, Summer 2 and Winter 2 and using coresponding values of viscosity. Figure 4.4 shows the velocity field due to wind only, in Summer 1.

The forces caused by the geostrophic currents and the ocean tilt can be calculated from the ocean height data using equations (2.4) and (2.5). The ocean height data at points on the same 250 km by 250 km grid system was also obtained from the Cold Regions Research and Engineering Laboratory (Hibler,1976). This data was generated from the long term Coachman's (1974) ocean height values, which is presented in Table 4.5. Two sets of pack ice velocities caused by ocean current and tilt were computed using different values of viscosity for summer and winter. Figures 4.5 and 4.6 show the velocity fields caused by ocean current and tilt in Summer 1.

In order to obtain the velocity field due to the combined forces of wind, currents and ocean tilt, we add all the velocity fields for each of the four seasons considered here. The combined velocity fields are shown in Figures 4.7 to 4.10 for Summer 1, Winter 1, Summer 2 and Winter 2, respectively.

The results of finite element analysis are compared with that of Fourier Transform method (Hibler,1976) and this comparison is shown in Figure 4.11. We note that

the results obtained from both methods agree with each other
in the middle of the basin. The differences near the boundary
are due to the fact that different boundary conditions have
been assumed for solution by the two methods. In the Fourier
Transform method, the solution repeats itself every 4000km in
the x and y direction. Slip type boundary conditions have
been assumed for the solution by finite element method. We
can also note from Figure 4.11 that the influence of different
boundary conditions extends upto a distance of approximately
750km. A comparison of pack ice drift velocity for Winter 1
pressure data is presented in Figure 4.12, when the slip and
no-slip boundary conditions are used. It can be noted that
the effect of boundary condition extends to a distance of 750km.

4.4 BOUNDARY ELEMENTS

The boundary conditions that can be imposed in the finite element solution are of two types: either the velocity or the stress in the normal and the tangential direction of the boundary can be prescribed. These boundary conditions may not be valid when the pack ice edge is moving away from the shore because the pack ice can not offer resistance in tension. The imposition of boundary condition must take care of the condition whether the pack ice edge is retreating from the shore or pushing against the shore. On the one hand, when the pack ice boundary is moving away from the shore, the boundary should be free to move without any stress imposed on it, on the other hand, when the pack ice boundary is pushing against the shore, the velocity normal to the shore must be zero and the tangential stress at the boundary must not be zero (preferably proportional to the normal pressure according to Coulomb yield criteria).

The above boundary conditions cannot be expressed linearly in terms of unknown velocity components of pack ice. Hence, an iterative procedure is followed to incorporate these non-linear boundary conditions with the help of boundary elements whose material properties (i.e., viscosities) can be changed as the iterative solution progresses. These boundary elements are long and not so wide elements placed at the boundary as shown in Figure 4.13. The velocity at the boundary nodes are made equal to zero. The material properties of these elements are first taken to be the same

as those in the domain. The nodal velocities of pack ice are
obtained and the stresses in the boundary elements are calcu-
lated. If a tensile stress exists in the direction normal to
the boundary, the element properties of the element are redu-
ced to a low value. It should be reduced to zero but this is
not done in order to avoid difficulties in numerical calcula-
tions. This procedure of obtaining the solution and checking
the stress in the boundary element to change its material pro-
perties is repeated a number of times until we get the same
solution as in the previous iterative step.

In Figure 4.13, the boundary elements have a width of
25km and length of 250km. The computer program was modified
to incorporate the above iterative procedure. The results of
computation of pack ice velocities due to wind stress in
Summer 1 is presented in Figure 4.14. Only two iterations
were necessary to obtain this result. The velocity field in
Figure 4.14 can be compared with the velocity field in Figure
4.4, in which a slip boundary condition is imposed. These
calculations were not repeated for all cases of driving forces
due to wind, currents and tilt, because we only want to demon-
strate the feasibility of such an iterative solution incorpo-
rating non-linear boundary condition.

4.5 STRAIT OF BELLE ISLE

The strait of Belle Isle lies between Newfoundland and Labrador (see Figure 4.15). The tidal streams in the strait move the pack ice to and fro, and the reversal in the direction of movement takes place every 5 or 6 hours. The Faculty of Engineering at Memorial University of Newfoundland has accumulated extensive data on the movement of ice in the form of time lapse photographs taken at Pointe Amour, Labrador, during the year 1974-75. It can be observed from these photographs that the pack ice reverses its direction, and some sort of eddys in pack ice are formed at the time of reversal of velocity.

An attempt is made to model the movement of pack ice due to water movement in the strait by the finite element method. It is reported in the Labrador and Hudson Bay Pilot (1965), issued by the Canadian Hydrographic Service, that the tidal streams attain an average velocity of 2 to 3 knots. The west-going stream reaches its maximum rate about 2 hours 35 minutes before high water at Harrington Harbour and the east-going stream at about the same interval before low water there.

The water movement actually experienced are the resultant of these tidal streams and of currents whose direction and rate are largely determined by meteorological conditions. The most unusual distribution of currents is an east-going current across the whole of the western entrance down to a depth of 20 fathoms (44 m) and a west-going current at greater depths.

Owing to the meteorological effects, the flow on any day may be either predominantly west-going or predominantly east-going, for the currents will quite commonly be strong enough to overcome the weaker of the two streams. The strongest east-going flows occur with the passage of a low pressure region over northern Quebec and the resultant of the current and the east-going tidal stream may have rates up to 3½ knots. The strongest west-going flows occur when an atmospheric pressure depression lies to the south of the strait and then the resultant current and west-going tidal stream may reach a rate of up to 5 knots on the northern side of the western entrance.

In order to model the movement of pack ice in the strait, we assume that the movement of water has a sinusoidal variation with a peak velocity of 3½ knots and a period of 12.5 hours. The interference of currents due to meteorological conditions is not taken into account because this is a first study on the movement of pack ice in the strait.

The strait of Belle Isle is discretized into finite size elements as shown in Figure 4.16. The forces acting on the pack ice are only due to the current. The Ekman angle in water is taken to be zero for this case. The system equations (3.4) are first order differential equations with respect to time. The integration is performed according to the 2nd order Runge-Kutta method with a time step of 300 to 900 seconds. The initial conditions are assumed to be zero. There

is a characteristic time associated with the first order system and the integration procedure remains stable as long as the integrating time step is smaller than the characteristic time.

The results of computation are presented in Figures 4.17 and 4.18. In Figures 4.17 the velocity of pack ice at the narrowest section is plotted at different time instants. The velocity remains constant throughout the section except near the boundary where a boundary layer effect exists. At the time of the velocity reversal, the velocity of pack ice near the shores reverses earlier than the main body of pack ice. This non-uniform pack ice motion can be observed in the time lapse photographs of ice in the strait. After a short time, the whole section starts to move together in the reversed direction. In Figures 4.18 the velocity of pack ice at the middle point of the narrowest section is plotted against time. Plots of water velocity with respect to time are also shown in Figures 4.18. It can be observed that the pack ice velocity lags behind the water velocity by a constant time. This time lag can be explained with the help of a simple model.

A mass m (kg) is attached to a linear damper of coefficient c (kg s^{-1}) (see Figure 4.19), such that the free end of the damper has a harmonic velocity of amplitude U and frequency ω. The resultant steady state velocity of the mass m can be obtained by solving the following equation:

$$\tau \dot{v} + v = U \sin \omega t \qquad (4.3)$$

where $\tau = \dfrac{m}{c}$ (s), the characteristic time of the system. The solution of the above equation can be written in the following form:

$$v(t) = V \sin (\omega t - \phi)$$

where $V = (1 + \tau^2 \omega^2)^{\frac{1}{2}} U$

$\tan \phi = \tau \omega$

$\phi = T \omega$ (T is time lag).

For small values of ϕ, we can conclude that the time lag T is equal to the characteristic time τ.

If we vary the values of bulk and shear viscosities in our model, we are essentially varying the damping coefficient c in the simplified model. As c increases, the characteristic time decreases. This trend is observed in the computation of pack ice velocity when the values of viscosity are changed as shown in Figures 4.18. If very large values of viscosity are used, the characteristic time would be very small, and it may not be worthwhile to integrate the first order system equation (3.4). In that case, the time varying term in equation (3.4) may be ignored due to smallness of inertial forces in comparison to the dissipative forces in the system. It is for this reason that steady state velocities are

calculated in the Arctic Basin where the values of viscosity
are very large.

From the time lapse photographs of the pack ice motion
in the strait of Belle Isle, it is possible to determine the
time instants when the reversal of ice motion took place. As
mentioned earlier, the movement of water in the strait is cor-
related to tide levels at Harington Harbor. We assume that
the water velocity in the strait is harmonic with respect to
time. With the help of the 'Labrador and Hudson Bay Pilot,
(1965)' and the 'Canadian Tide and Current Tables (1974, 1975,
1976)', we have been able to determine the time instants of
water velocity reversals in the strait on those windless days
when the pack ice motion was photographed. It is found that
the time lag between the reversals of water velocity and that
of the pack ice is approximately 18 to 29 minutes when there
is no wind.

The theoretical model can be made to simulate the motion
of pack ice in the strait by properly choosing the values of
viscosity. Computations are performed for three different
values of viscosity and the following table gives the charac-
teristic time coresponding to each value of viscosity used.

η, ζ (kg s^{-1})	τ (seconds)
0.6×10^5	1980
1.2×10^5	1140
2.4×10^5	390

The approach of parameterizing the model is to choose those values of bulk and shear viscosities which give theoretical time lag equal to the actual time lag.

The above model describes the motion of pack ice in the strait for a sinusoidal variations of water velocity. For the determination of pack ice motion due to different meteorological conditions, one must first model the movement of water through the strait taking many factors into account, e.g., effect of the Moon and the Sun, atmospheric pressure, bottom topography of the strait, etc.

CHAPTER 5

DISCUSSION AND CONCLUSION

A number of investigators have employed viscous sea ice drift models over several years (Doronin,1970; Laikhtman,1962; Campbell,1965; Hibler,1974). In all those models, the stress transmitted through the sea ice cover on the geophysical scale is considered to be a single valued function, usually linear, of the strain rate tensor. In order to make use of a viscous type model, it is necessary to have some way of parameterizing the viscosity as a function of the state of ice. Doronin (1970) used a relationship between compactness and viscosity. A simpler approach is to parameterize the viscosity to a first approximation as a function of the thermodynamics of the ice cover; in particular the growth rate of ice as used by Hibler (1976b).

The finite element formulation of a viscous sea ice mdoel has been accomplished in this thesis for both steady and non-steady drift velocity of pack ice. The working of a finite element computer program is checked by comparing its solution for a hypothetical pressure variations with the exact solution obtained by Fourier Transform method (Hibler,1976b). Four sets of pack ice velocity field in the Arctic Basin are

computed and plotted using six monthly averaged atmospheric
pressure data and long term ocean height.

The slip type boundary condition is not strictly valid
when pack ice pushes against the shore. When pack ice recedes
from the shore, free (ie. zero stress) boundary condition
must be imposed. This non-linear behavior of boundary condi-
tions has been incorporated in the iterative procedure by
introducing boundary elements whose properties change accor-
ding to the state of stress in the element.

When the forces acting on the pack ice change rapidly
and the response time for the ice to those forces is large,
non-steady ice velocity has to be computed. This has been
done for the to and fro motion of pack ice in the strait of
Belle Isle due to tidal streams and currents. For a harmonic
variation of tidal stream velocity with respect to time, the
pack ice velocity is also harmonic with a time lag with respect
to the water velocity. The time lag in the model can be adju-
sted by varying the values of bulk and shear viscosities, and
it can be matched to the actual time lag which has been deter-
mined in a few instances with the help of time lapse photogra-
phs of ice motion and the tide tables.

SCOPE FOR FURTHER STUDY

This work has been the first step towards the finite
element formulation of the viscous model for sea ice. More
detailed computations of the pack ice velocity field can be
accomplished with better atmospheric pressure data and by
taking non-linear boundary conditions into account over an
irregular domain.

The pack ice drift in the strait of Belle Isle is
strongly influenced by the water movement in the strait
which is the resultant of the tidal streams and the currents
affected by the Moon, the Sun and the meteorological cond-
itions. Further studies on the pack ice drift in the strait
should include all the factors influencing the water move-
ment. This would also shed some light on the question
whether there is any net import or export of energy from
the Gulf of St.Lawrence through the strait of Belle Isle.

REFERENCES

Brennecke, W. 1921. Der Ozeanographischen Arbeiten Der Deuts chen Antarktischen Expedition 1911-1912. *Deutsche Seewarte Archiv*, Vol.39. No.1. pp.216; Hamburg.

Buynitskiy, V. Kh. 1951. The formation and drift of the ice cover in the Arctic Basin. *Trudy of the 'Sedov' 'Expedition'* Vol.4. Leningrad.

Campbell, W.J. 1965. The wind driven circulation of ice and water in a polar ocean, *Journal of Geophysical Research*, Vol. 70. No.14. pp. 3279-3301.

Canadian Tide and Current Tables, 1974,1975 and 1976.

Coachman, L.K. and Aagard, K. 1974. Physical oceanography of the Arctic and sub Arctic seas. *Marine Geology and Oceano-graphy of the Arctic seas*, edt. Y. Herman, Springer Verlag, Newyork.

Colony, R. and Rash, P. 1975. Drift paths in the Arctic Ocean *AIDJEX Bull.*28.

Coon, M.D. 1972. Mechanical behavior of compacted Arctic floes. *Offshore Technology Conference, Houston, Texas*, paper No. O.T.C. 1684.

Coon, M.D., Maykut, G.A., Pritchard, R.S., Rothrock, D.A. and Thorndike, A.S. 1974. Modeling the pack ice as an elastic-plastic material. *AIDJEX Bull*.24. pp.1-105.

Desai, C. and Abel, J. 1972. *Introduction to Finite Element Method.* Van Nostrand Reinhold Co. Newyork.

Doronin, Yu. P. 1970. (English Transl.) On a Method of calcu-lating compactness and drift of ice floes. *AIDJEX Bull*.3. pp.22-39.

Drogoitsev, D.A. 1956. Zones of compression and rarefaction of ice in the atmospheric pressure field. *English Transl. by Defence Research Board Can.*,T 264 R.

Dunbar, M. and Wittman, W. 1963. Some features of ice move-ment in the Arctic Basin. *Proc. Arctic Basin symp.* 90-104, Washington D.C., Arctic Inst. N.Am.

Evans, R.J. 1970. Notes on possible constitutive law for Arctic sea. *AIDJEX Bull*.2. pp.13-17.

Glen, J.W. 1970. Thoughts on a viscous model for sea ice. AIDJEX Bull.2. pp.18-27.

Haggerty, G.B. 1972. Elementary Numerical Analysis with programming. Allyn and Bacon, Inc. Boston.

Hibler, W.D., Ackley, S.F., Crowder,W.K., Mckim,H.L. and Anderson,D.M. 1974a. Analysis of shear zone ice deformation in the Beaufort sea using satellite imagery. The coast and shelf of Beaufort sea, ed. J.C.Reed.

Hibler,W.D. 1974. Differential sea ice drift.II. Comparison of meoscale strain measurements with linear drift theory predictions. Journal of Glaciology, Vol.13.,No.69. pp.22-39.

Hibler,W.D. and Tucker,W.B. 1976. Seasonal variations in apparent sea ice viscosity on the geophysical scale. Internal Note from CRREL.

Hibler,W.D. 1976. Private communications.

Huebner, K.H. 1975, Finite element method for Engineers, John Wiley and sons, Newyork.

The Labrador and Hudson Bay Pilot, 1965.

Laikhtman,D.L. 1961. Fizika Progranichnogo Sloya Atmosfery. (English Translation published by U.S.Dept. of commerce, Washington,1964)

Matsuoka, K. 1972. The mechanics of fracture of sea ice in leads. Masters thesis, University of Washington.

Maykut,G.A. and Thorndike,A.S. 1973. An approach to coupling the dynamics and the thermodynamics of Arctic sea ice.AIDJEX Bull. 21. pp.23-29.

Nansen,F. 1902. The oceanography of North Polar Basin. The Norwegian Polar Expedition 1893-1896. Scientific Results 3 pp. 357-386. Christiana (Oslo): A.W.Brogger.

Neumann, G. and Pierson,W.J. 1966. Principles of Physical Oceanography. Prentice-hall Inc. Englewood Cliffs N.J.

Nikiforov,Ye.G. 1957. A change in the concentration of ice cover in connection with its dynamics.(Transl. by Am. Met. Soc. NTIS No. AD232204.

Nye,J.F. and Thomas,D.R. 1974. The use of satellite photographs to give the movement and deformation of sea ice. AIDJEX Bull.27. pp.1-21.

Nye, J.F. 1973a. The meaning of a two dimensional strain rate in a floating ice cover. AIDJEX Bull.21. pp. 9-17.

Nye,J.F. 1974. Three notes on the theory of sea ice movement. AIDJEX Bull.23. pp.37-51.

Parmerter,R.R. and Coon,M.D.1973. On the mechanics of pressure ridge formation in sea ice. Proc. of Offshore Technology Conference, Houston, Texas. Vol.1. pp.733-742.

Parmerter,R.R. 1974a. Dimensionless strength parameters for floating ice sheets. AIDJEX Bull.23. pp.83-95.

Parmerter,R.R. 1974b. A mechanical model of rafting. AIDJEX Bull.23. pp.97-115.

Pritchard, R.S. 1974. Elastic strain in the AIDJEX sea ice model. AIDJEX Bull.27. pp.45-62.

Rothrock,D.A. 1975. The mechanical behavior of pack ice. Annual Review of Earth and Planetary sciences. Vol.3. pp.317-342.

Rothrock,D.A. 1975. The steady drift of an incompressible Arctic ice cover. Journal OF Geophysical Research. Vol.80. No.3. pp.387-397.

Rothrock,D.A. 1973. The steady drift of an incompressible Arctic ice cover. AIDJEX Bull.21. pp.49-77.

Sverdrup, H.U. 1928. Die Eisdrift im Weddelmer. Ann. d,Hyder. U. Marit. Meteorol, Vol.56. pp.265.

Timokov,L.A. 1970. (English Transl.) Dynamics and kinematics of ice floes. AIDJEX Bull.3. pp.65-79.

APPENDIX A

TRIANGULAR ELEMENT FORMULATION

A brief discussion on the development of a triangular finite element is presented here. Figure A-1 shows a typical triangular element with nodes 1, 2, 3 numbered in anticlockwise direction. The following are the interpolation functions for the velocity components within the triangular element:

$$u = \alpha_1 + \alpha_2 x + \alpha_3 y$$
$$v = \alpha_4 + \alpha_5 x + \alpha_6 y \tag{A.1}$$

We can write the above equations in the following form:

$$\begin{bmatrix} u \\ v \end{bmatrix} = \begin{bmatrix} 1 & x & y & 0 & 0 & 0 \\ 0 & 0 & 0 & 1 & x & y \end{bmatrix} \begin{bmatrix} \alpha_1 \\ \alpha_2 \\ \alpha_3 \\ \alpha_4 \\ \alpha_5 \\ \alpha_6 \end{bmatrix} \tag{A.2}$$

In order to express velocity components in terms of the values of velocity components at the nodes, we eliminate the coefficients α's by the use of the following equations:

$$\begin{bmatrix} u_1 \\ u_2 \\ u_3 \\ v_1 \\ v_2 \\ v_3 \end{bmatrix} = \begin{bmatrix} 1 & x_1 & y_1 & 0 & 0 & 0 \\ 1 & x_2 & y_2 & 0 & 0 & 0 \\ 1 & x_3 & y_3 & 0 & 0 & 0 \\ 0 & 0 & 0 & 1 & x_1 & y_1 \\ 0 & 0 & 0 & 1 & x_2 & y_2 \\ 0 & 0 & 0 & 1 & x_3 & y_3 \end{bmatrix} \begin{bmatrix} \alpha_1 \\ \alpha_2 \\ \alpha_3 \\ \alpha_4 \\ \alpha_5 \\ \alpha_6 \end{bmatrix} \qquad (A.3)$$

where u_i and v_i ($i=1,3$) are the nodal velocities in the
x and y directions, and x_i and y_i are the coordinates of the
nodal points 1,2 and 3. By inverting the above set of equa-
tions and substituting for the coefficients α's in equation
(A.2), we get

$$\begin{bmatrix} u \\ v \end{bmatrix} = \frac{1}{2A} \begin{bmatrix} 1 & x & y & 0 & 0 & 0 \\ 0 & 0 & 0 & 1 & x & y \end{bmatrix} \begin{bmatrix} 2A_{23} & 2A_{31} & 2A_{12} & 0 & 0 & 0 \\ b_1 & b_2 & b_3 & 0 & 0 & 0 \\ a_1 & a_2 & a_3 & 0 & 0 & 0 \\ 0 & 0 & 0 & 2A_{23} & 2A_{31} & 2A_{12} \\ 0 & 0 & 0 & b_1 & b_2 & b_3 \\ 0 & 0 & 0 & a_1 & a_2 & a_3 \end{bmatrix} \begin{bmatrix} u_1 \\ u_2 \\ u_3 \\ v_1 \\ v_2 \\ v_3 \end{bmatrix}$$

$$(A.4)$$

where $A_{ij} = x_i y_j - y_i x_j$

$a_1 = x_3 - x_2 \qquad a_2 = x_1 - x_3 \qquad a_3 = x_2 - x_1$

$b_1 = y_2 - y_3 \qquad b_2 = y_3 - y_1 \qquad b_3 = y_1 - y_2$

$2A = a_3 b_2 - a_2 b_3 = a_1 b_3 - a_3 b_1 = a_2 b_1 - a_1 b_2$

It is convenient to express equation (A.4) in terms of
the natural coordinates of the triangle as follows:

$$\begin{bmatrix} u \\ v \end{bmatrix} = \begin{bmatrix} L_1 & L_2 & L_3 & 0 & 0 & 0 \\ 0 & 0 & 0 & L_1 & L_2 & L_3 \end{bmatrix} \begin{bmatrix} u_1 \\ u_2 \\ u_3 \\ v_1 \\ v_2 \\ v_3 \end{bmatrix} = [N]\{q_e\} \qquad (A.5)$$

where $L_1 = \frac{1}{2A}(2A_{23} + b_1x + a_1y)$

$L_2 = \frac{1}{2A}(2A_{11} + b_2x + a_2y)$

$L_3 = \frac{1}{2A}(2A_{12} + b_3x + a_3y)$

$L_1 + L_2 + L_3 = 1$

$\{q_e\}$ is the generalised nodal velocity vector.

There is a convenient formula for integrating the natural coordinates over the area of a triangular element, and it is given below:

$$\iint_{A_\Delta} L_1^p \ L_2^q \ L_3^r \ dA = \frac{p! \ q! \ r!}{(p+q+r+2)!} \ 2A \qquad (A.6)$$

By differentiating equation (A.5), we obtain the following expression for the strain rate components:

$$\{\dot{\varepsilon}\} = \begin{bmatrix} u,_x \\ v,_y \\ u,_y + v,_x \end{bmatrix} = \frac{1}{2A} \begin{bmatrix} b_1 & b_2 & b_3 & 0 & 0 & 0 \\ 0 & 0 & 0 & a_1 & a_2 & a_3 \\ a_1 & a_2 & a_3 & b_1 & b_2 & b_3 \end{bmatrix} \begin{bmatrix} u_1 \\ u_2 \\ u_3 \\ v_1 \\ v_2 \\ v_3 \end{bmatrix} = [B]\{q_e\} \qquad (A.7)$$

There are four types of expressions in the functional (3.2) and we shall deal with them one by one.

Type 1.

The energy dissipation due to water drag, the rate of work done by Coriolis force and the rate of change of kinetic energy can be expressed by an expression of the following form:

$$\iint \frac{1}{2} \begin{bmatrix} u & v \end{bmatrix} \begin{bmatrix} P_{11} & P_{12} \\ P_{21} & P_{22} \end{bmatrix} \begin{bmatrix} u \\ v \end{bmatrix} dA \tag{A.8}$$

Substituting equation (A.5) into the above expression, we have

$$\frac{1}{2} \iint \begin{bmatrix} u_1 & u_2 & u_3 & v_1 & v_2 & v_3 \end{bmatrix} \begin{bmatrix} L_1 & 0 \\ L_2 & 0 \\ L_3 & 0 \\ 0 & L_1 \\ 0 & L_2 \\ 0 & L_3 \end{bmatrix} \begin{bmatrix} P_{11} & P_{12} \\ P_{21} & P_{22} \end{bmatrix} \begin{bmatrix} L_1 & L_2 & L_3 & 0 & 0 & 0 \\ 0 & 0 & 0 & L_1 & L_2 & L_3 \end{bmatrix} \begin{bmatrix} u_1 \\ u_2 \\ u_3 \\ v_1 \\ v_2 \\ v_3 \end{bmatrix} dA$$

$$= \frac{1}{2} \{q_e\}^t [K_p] \{q_e\} \tag{A.9}$$

where $[K_p] = A \begin{bmatrix} P_{11}[S] & P_{12}[S] \\ P_{21}[S] & P_{22}[S] \end{bmatrix}$ and $[S] = \begin{bmatrix} \frac{1}{6} & \frac{1}{12} & \frac{1}{12} \\ \frac{1}{12} & \frac{1}{6} & \frac{1}{12} \\ \frac{1}{12} & \frac{1}{12} & \frac{1}{6} \end{bmatrix}$

The mass matrix can be derived from the above term and it is written as follows:

$$[M_e] = \begin{bmatrix} m[S] & [0] \\ [0] & m[S] \end{bmatrix} \qquad (A.10)$$

Type 2.

If the forces due to wind, ocean currents and ocean tilt are known, we can group the second, third and fourth terms in the functional as follows:

$$\iint [u \quad v] \begin{bmatrix} F_x(x,y) \\ F_y(x,y) \end{bmatrix} dA \qquad (A.11)$$

The functions $F_x(x,y)$ and $F_y(x,y)$ can be obtained from the atmospheric pressure data and the ocean height data by the use of equations (2.3 to 2.6). We assume that F_x and F_y vary linearly with respect to x and y within the triangular element, and we can write

$$\begin{bmatrix} F_x \\ F_y \end{bmatrix} = \begin{bmatrix} L_1 & L_2 & L_3 & 0 & 0 & 0 \\ 0 & 0 & 0 & L_1 & L_2 & L_3 \end{bmatrix} \begin{bmatrix} F_{x1} \\ F_{x2} \\ F_{x3} \\ F_{y1} \\ F_{y2} \\ F_{y3} \end{bmatrix} \qquad (A.12)$$

where F_{xi} and F_{yi} (i=1 to 3) are the values of F_x and F_y at the nodes of the element. Now we can write the expression (A.11) in the following manner:

$$\iint \begin{bmatrix} u_1 & u_2 & u_3 & v_1 & v_2 & v_3 \end{bmatrix} \begin{bmatrix} L_1 & 0 \\ L_2 & 0 \\ L_3 & 0 \\ 0 & L_1 \\ 0 & L_2 \\ 0 & L_3 \end{bmatrix} \begin{bmatrix} L_1 & L_2 & L_1 & 0 & 0 & 0 \\ 0 & 0 & 0 & L_1 & L_2 & L_3 \end{bmatrix} \begin{bmatrix} F_{x_1} \\ F_{x_2} \\ F_{x_3} \\ F_{y_1} \\ F_{y_2} \\ F_{y_3} \end{bmatrix} dA$$

$$= \{q_e\}^t \{Q_e\} \tag{A.13}$$

where $\{Q_e\} = A \begin{bmatrix} \dfrac{F_{x1}}{6} + \dfrac{F_{x2}}{12} + \dfrac{F_{x3}}{12} \\[2ex] \dfrac{F_{x1}}{12} + \dfrac{F_{x2}}{6} + \dfrac{F_{x3}}{12} \\[2ex] \dfrac{F_{x1}}{12} + \dfrac{F_{x2}}{12} + \dfrac{F_{x3}}{6} \\[2ex] \dfrac{F_{y1}}{6} + \dfrac{F_{y2}}{12} + \dfrac{F_{y3}}{12} \\[2ex] \dfrac{F_{y1}}{12} + \dfrac{F_{y2}}{6} + \dfrac{F_{y3}}{12} \\[2ex] \dfrac{F_{y1}}{12} + \dfrac{F_{y2}}{12} + \dfrac{F_{y3}}{6} \end{bmatrix}$

Type 3.

The rate of energy dissipation into the material deformation is expressed by the following expression in the functional (3.2):

$$\frac{1}{2}\iint [u_{,x} \quad v_{,y} \quad u_{,y}+v_{,x}]\begin{bmatrix} \zeta+\eta & \zeta-\eta & 0 \\ \zeta-\eta & \zeta+\eta & 0 \\ 0 & 0 & \eta \end{bmatrix}\begin{bmatrix} u_{,x} \\ v_{,y} \\ u_{,y}+v_{,x} \end{bmatrix} dA \quad (A.14)$$

$$= \frac{1}{2}\iint \{\dot{\epsilon}\}^t [R]\{\dot{\epsilon}\} \, dA$$

$$= \frac{1}{2}\iint \{q_e\}^t [B]^t [R][B]\{q_e\} \, dA$$

$$= \frac{1}{2}\{q_e\}^t [K_e]\{q_e\}$$

where $[K_e] = \dfrac{1}{4A}\begin{bmatrix} b_1 & 0 & a_1 \\ b_2 & 0 & a_2 \\ b_3 & 0 & a_3 \\ 0 & a_1 & b_1 \\ 0 & a_2 & b_2 \\ 0 & a_3 & b_3 \end{bmatrix}\begin{bmatrix} \zeta+\eta & \zeta-\eta & 0 \\ \zeta-\eta & \zeta+\eta & 0 \\ 0 & 0 & \eta \end{bmatrix}\begin{bmatrix} b_1 & b_2 & b_3 & 0 & 0 & 0 \\ 0 & 0 & 0 & a_1 & a_2 & a_3 \\ a_1 & a_2 & a_3 & b_1 & b_2 & b_3 \end{bmatrix}$

In the derivation of above expressions, we have made use of equations (A.7). The matrix [R] represents the constitutive relations in terms of moduli of viscosity.

Type 4.

The line integral term in the functional (3.2) represents the rate of work done by the prescribed boundary stresses, and it can be presented in the following form:

$$\int_{S_f} \begin{bmatrix} u_n & u_t \end{bmatrix} \begin{bmatrix} \sigma_{nn} \\ \tau_{nt} \end{bmatrix} ds = \int_{S_f} \begin{bmatrix} u & v \end{bmatrix} \begin{bmatrix} X \\ Y \end{bmatrix} ds \qquad (A.15)$$

where $X = \sigma_{nn} \cos\theta - \tau_{nt} \sin\theta$

$\qquad\quad Y = \sigma_{nn} \sin\theta + \tau_{nt} \cos\theta$

and θ is the angle between the outward normal and x-axis.

Suppose that the element (e) forms part of the boundary curve S_f as shown in Figure A-2 and the nodes i and j lie on the boundary where the stresses are prescribed. We can evaluate the boundary integral in equation (A.15) as sum of integrals over segments, such as i-j in Figure A-2. We can express the velocity components at the boundary in terms of values of velocities (u_i, u_j, v_i and v_j) at nodes i and j as follows:

$$\begin{bmatrix} u \\ v \end{bmatrix} = \begin{bmatrix} (1-\frac{s}{l_{ij}}) & \frac{s}{l_{ij}} & 0 & 0 \\ 0 & 0 & (1-\frac{s}{l_{ij}}) & \frac{s}{l_{ij}} \end{bmatrix} \begin{bmatrix} u_i \\ u_j \\ v_i \\ v_j \end{bmatrix} \qquad (A.16)$$

where s and l_{ij} are the arc-lengths defined in Figure A-2. If we assume that X and Y are also linearly varying along the boundary segment i-j, we can specify X and Y in terms

of their nodal values $(X_i, X_j, Y_i$ and $Y_j)$ in the following form:

$$\begin{bmatrix} X \\ Y \end{bmatrix} = \begin{bmatrix} (1-\frac{s}{1_{ij}}) & \frac{s}{1_{ij}} & 0 & 0 \\ 0 & 0 & (1-\frac{s}{1_{ij}}) & \frac{s}{1_{ij}} \end{bmatrix} \begin{bmatrix} X_i \\ X_j \\ Y_i \\ Y_j \end{bmatrix}$$ (A.17)

Substituting equations (A.16) and (A.17) into equation (A.15), we have

$$\int_{S_f} [u \quad v] \begin{bmatrix} X \\ Y \end{bmatrix} ds = [u_i \quad u_j \quad v_i \quad v_j] \begin{bmatrix} 1_{ij}(\frac{X_i}{3} + \frac{X_j}{6}) \\ 1_{ij}(\frac{X_i}{6} + \frac{X_j}{3}) \\ 1_{ij}(\frac{Y_i}{3} + \frac{Y_j}{6}) \\ 1_{ij}(\frac{Y_i}{6} + \frac{Y_j}{3}) \end{bmatrix}$$ (A.18)

$$= \{q_b\}^t \{Q_b\}$$

where $\{q_b\}$ and $\{Q_b\}$ are the generalised velocity and force vectors at the boundary.

The functional in equation (3.2) can be evaluated over each element of the discretized system according to the procedure given above for the four types of expressions in the functional. This leads to the development of element matrices and generalised force vectors which are assembled in the usual

manner to give rise to an expression of the functional Π for the whole system.

$$\Pi = \Sigma \; \Pi_e = \Sigma \left[\tfrac{1}{2}\{q_e\}^t[K_p]\{q_e\} - \tfrac{1}{2}\{q_e\}^t[K_e]\{q_e\} \right.$$
$$\left. - \tfrac{1}{2}\{q_e\}^t[M_e]\{\dot{q}_e\} + \{q_e\}^t\{Q_e\} + \{q_b\}^t\{Q_b\} \right]$$

or $\quad \Pi = -\tfrac{1}{2}\{q\}^t[K]\{q\} - \tfrac{1}{2}\{q\}^t[M]\{\dot{q}\} + \{q\}^t\{Q\}$ $\qquad$ (A.19)

where the matrices [K] and [M] and the vectors {q} and {Q} refer to the entire discretized system after assembling the element matrices and vectors according to the usual procedure of assembly in the finite element method.

The first variation of the functional given in equation (A.19) is written as follows:

$$\delta\Pi = \delta\{q\}^t\left[-[K]\{q\} - [M]\{\dot{q}\} + \{Q\}\right] = 0 \qquad (A.20)$$

if $\delta\{q\}$ is to be arbitrary, the equation (A.20) gives the following system equations:

$$[M]\{\dot{q}\} + [K]\{q\} = \{Q\} \qquad\qquad (A.21)$$

The above first order differential equation with respect to time can be integrated by any one of the numerical integration procedure.
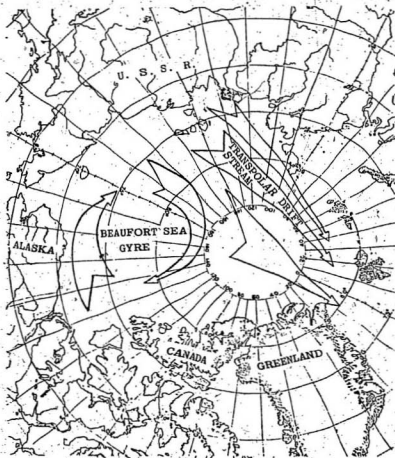
APPENDIX B

Figure 1.1   The pattern of Beaufort Sea gyre and
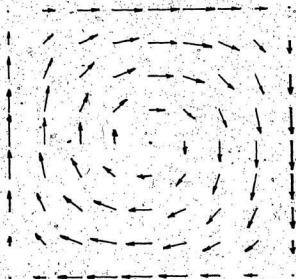   transpolar drift stream in the Arctic
            Ocean.

Figure 4.1 Wind velocity field due to hypothetical
atmospheric pressure variation.
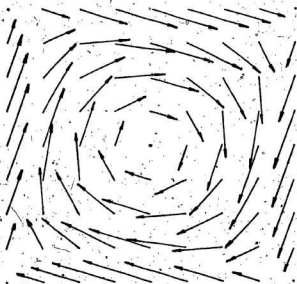Scale: 7.5 m s^{-1} per grid length.

Figure 4.2a Pack ice velocity field for
$\zeta = \eta = 2.0 \times 10^{10}$ kg s^{-1}
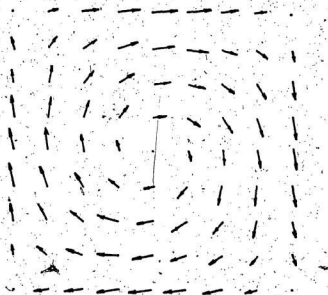Scale: 0.08 m s^{-1} per grid length

Figure 4.2b Pack ice velocity field for
$\zeta = \eta = 4.0 \times 10^{11}$ kg s^{-1}
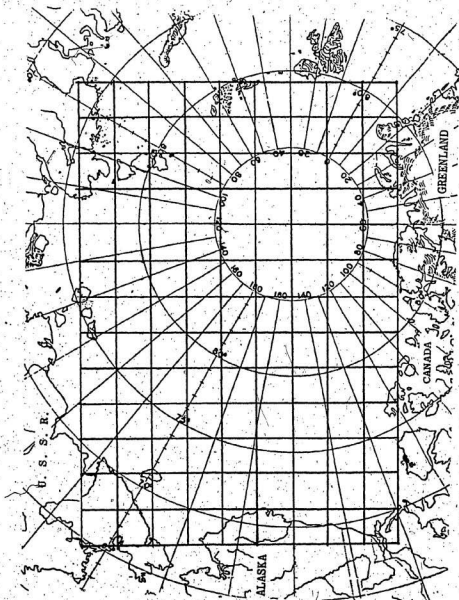Scale: 0.08 m s^{-1} per grid length
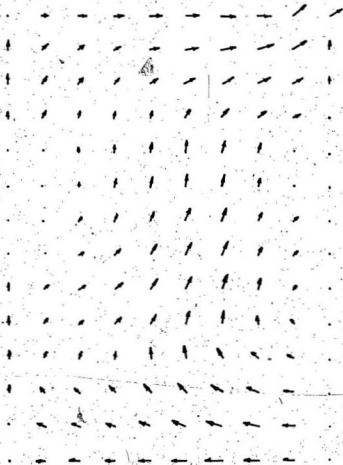
Figure 4.3   Discretization of the Arctic Basin.

Figure 4.4   Pack ice velocity field due to wind stresses only in
Summer 1. ($\zeta = \eta = 4.0 \times 10^{10}$ kg s^{-1})
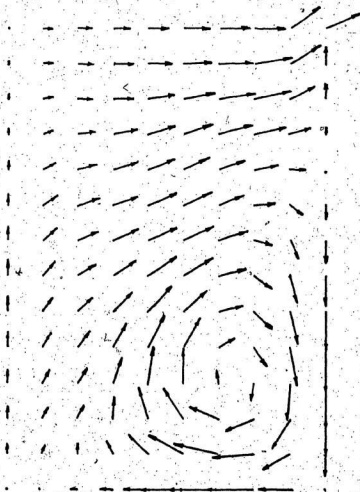Scale: 0.08 m s^{-1} per grid length.

Figure 4.5. Pack ice velocity field due to ocean currents only
$(\zeta = \eta = 4.0 \times 10^{10} \text{ kg s}^{-1})$
Scale: 0.01 m s^{-1} per grid length.
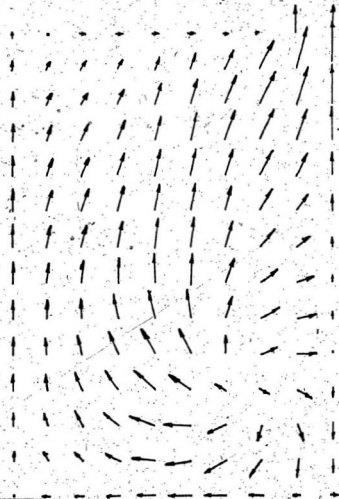
Figure 4.6   Pack ice velocity field due to ocean tilt only.
($\zeta = \eta = 4.0 \times 10^{11}$ kg.s^{-1}).
Scale: 0.0075 m s^{-1} per grid length.

Figure 4.7 Pack ice velocity field due to wind, ocean currents and ocean tilt in Summer 1. ($\zeta = \eta = 4.0 \times 10^{10}$ kg s^{-1}) Scale: 0.08 m s^{-1} per grid length.

Figure 4.8   Pack ice velocity field due to wind, ocean currents and ocean tilt in Winter 1. ($\zeta = \eta = 3.0 \times 10^{11}$ kg s^{-1}) Scale: 0.08 m s^{-1} per grid length
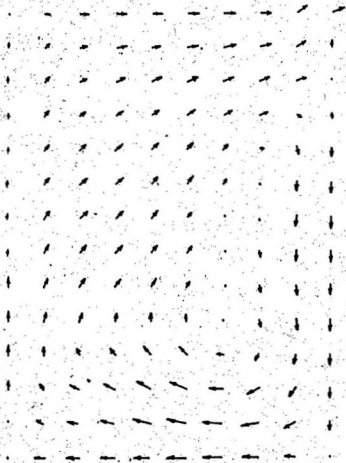
Figure 4.9   Pack ice velocity field due to wind, ocean currents and ocean tilt in Summer 2. ($c = \eta = 4.0 \times 10^{10}$ kg s^{-1}) Scale: 0.08 m s^{-1} per grid length.
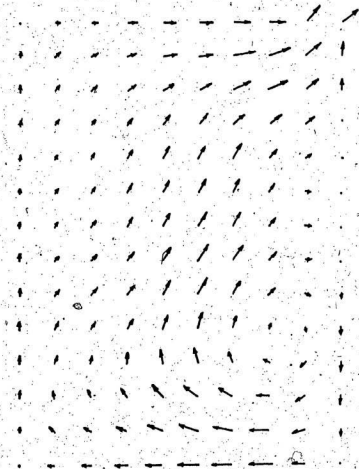
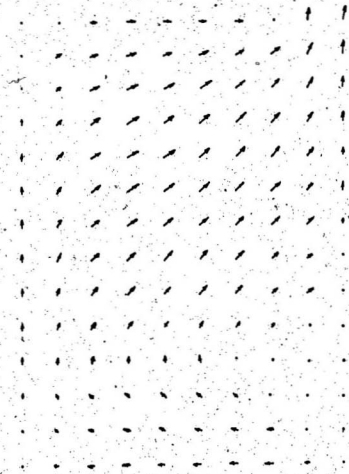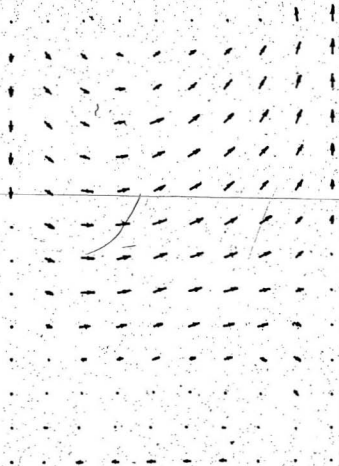Figure 4.10 Pack ice velocity field due to wind, ocean currents and ocean tilt in Winter 2. ($\zeta = \eta = 3.0 \times 10^{11}$ kg s^{-1}) Scale: 0.08 m s^{-1} per grid length.

P.E. Method /. · F.T. Method
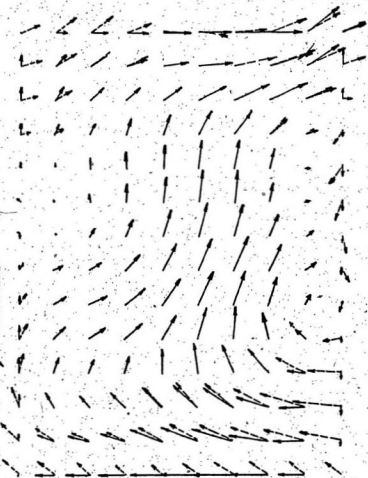
Figure 4.11 A comparison between the results of finite element method and Fourier Transform method.($\zeta = \eta = 4 \times 10^{10}$ kg s^{-1})
Scale: 0.025 m s^{-1} per grid length.

Slip boundary condition / No slip boundary condition
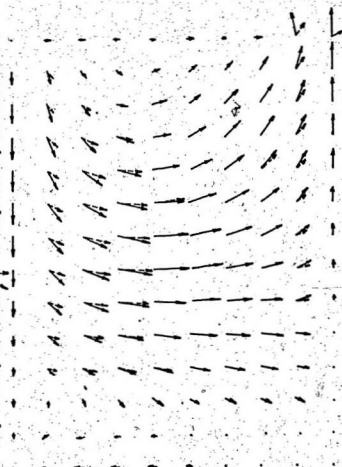
Figure 4.12 Effect of slip and no slip boundary conditions on the solution within the domain. ($\epsilon = m = 3 \times 10^{-1}$ kg s^{-1}). Scale: 0.025 m s^{-1} per grid length.

Figure 4.13 Discretization of the Arctic Basin with boundary elements.
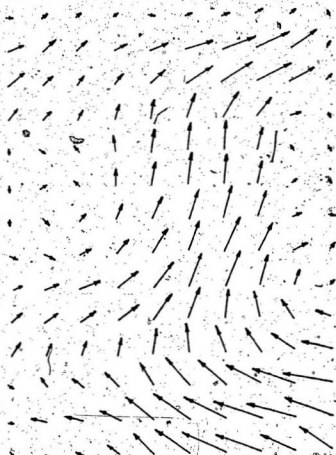
Figure 4.14 Pack ice velocity field due to wind stresses only
in Summer 1 with the incorporation of non-linear
boundary conditions. ($\zeta = \eta = 4.0 \times 10^{10}$ kg s^{-1})
Scale: 0.025 m s^{-1} per grid length.

N

LABRADOR

Pointe Amour   Strait of Belle Isle

Atlantic Ocean

Harrington
Harbour

Gulf of St. Lawrence

NEWFOUNDLAND

St. John's
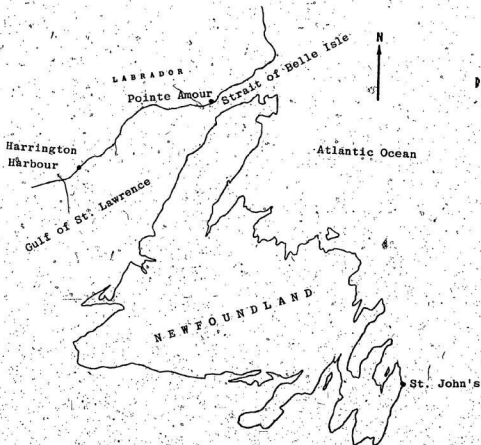
Figure 4.15 Strait of Belle Isle.
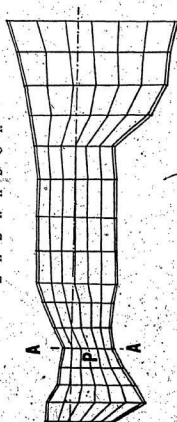
Figure 4.16 Discretization of strait of Belle Isle.

Figure 4.17 Velocity profiles at the narrowest section of the strait for different values of the viscosity parameter.
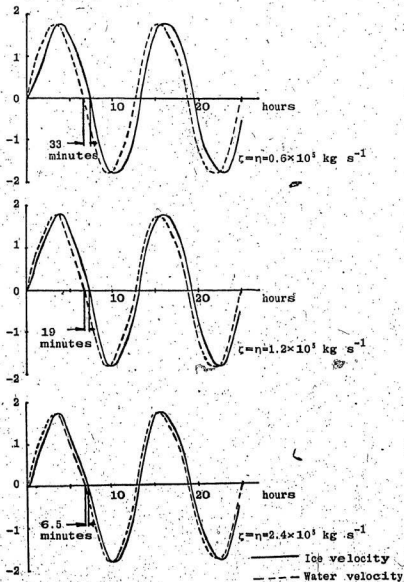
Figure 4.18 Plot of pack ice and water velocities with respect to time for different viscosity parameters.
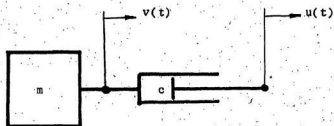
Figure 4.19   Simplified model
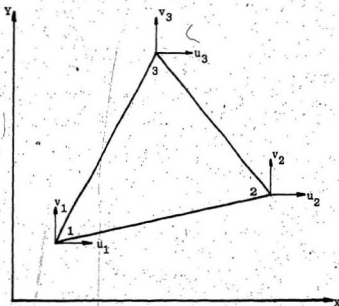
Figure A-1. Triangular finite element.
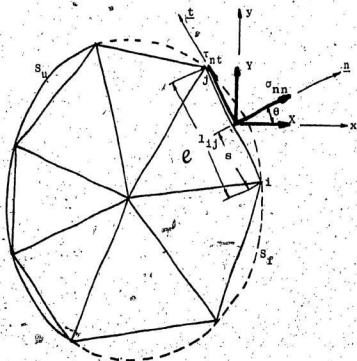
Figure A-2   Boundary stresses

Table 411   Atmospheric Pressure in Summer 1 (millibars)

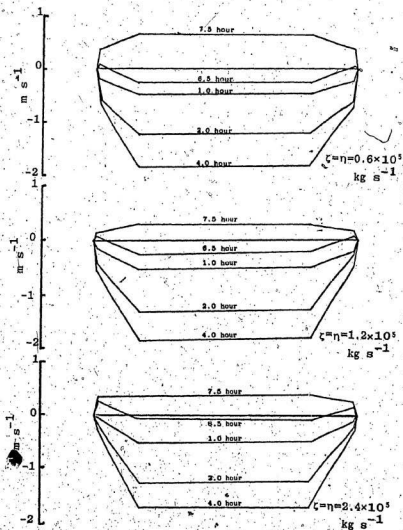|										
1012.14	1012.26	1012.12	1011.99	1011.84	1011.85	1011.69	1011.79	1011.64	1012.18	
1012.76	1012.89	1013.18	1013.13	1012.82	1012.39	1012.19	1012.58	1012.67	1012.25	
1015.45	1015.12	1014.94	1014.68	1014.28	1013.93	1013.38	1013.10	1012.98	1012.91	1012.83
1015.71	1015.33	1015.12	1014.56	1014.10	1013.57	1013.38	1012.98	1012.98	1012.63	
1015.32	1015.05	1014.94	1014.07	1013.04	1013.25	1013.14	1013.11	1012.88	1012.42	
1015.05	1016.05	1015.58	1014.76	1013.84	1013.10	1012.69	1012.98	1012.74	1012.36	
1015.05	1015.71	1015.32	1014.51	1013.60	1012.99	1012.40	1012.26	1012.54	1012.34	
1014.45	1015.35	1015.06	1014.31	1013.48	1013.08	1012.54	1012.27	1012.36	1012.40	
1015.07	1015.45	1015.35	1014.57	1013.19	1012.98	1012.62	1012.43	1012.33	1012.53	
1015.47	1015.93	1015.57	1014.49	1013.69	1013.18	1012.92	1012.64	1012.45	1012.64	
1015.44	1015.51	1014.95	1014.81	1014.26	1013.52	1013.02	1012.79	1012.62	1012.57	
1015.03	1013.66	1014.95	1014.39	1014.04	1013.79	1013.16	1012.86	1012.20	1012.21	
1014.06	1012.91	1013.36	1013.38	1013.15	1013.14	1012.91	1012.90	1012.14	1011.78	
1013.12	1012.33	1012.85	1012.19	1012.45	1012.74	1012.85	1012.42	1011.29	1011.10	

Table 4.2 Atmospheric Pressure in Winter 1 (millibars)

1020.0V	1019.51	1018.90	1018.64	1016.38	1016.11	1017.57	1017.26	1017.11	1016.52
1020.23	1019.92	1019.63	1019.24	1018.07	1018.43	1018.14	1018.52	1018.88	1018.40
1020.31	1020.38	1020.20	1019.92	1019.68	1019.31	1019.00	1018.99	1019.15	1019.35
1020.7	1020.50	1020.22	1020.08	1019.77	1019.37	1019.18	1019.10	1019.07	1019.38
1019.90	1000.13	1019.44	1019.73	1019.36	1018.92	1018.05	1018.40	1018.61	1018.98
1019.37	1019.72	1019.71	1019.36	1018.95	1018.56	1019.26	1018.19	1018.46	1018.84
1018.64	1019.98	1018.98	1018.59	1018.26	1017.98	1017.91	1017.48	1017.81	1018.27
1017.75	1018.29	1018.23	1017.91	1017.35	1016.83	1017.04	1017.00	1017.34	1017.67
1017.24	1018.19	1018.08	1017.52	1016.60	1016.17	1016.15	1016.12	1016.43	1016.77
1017.19	1018.04	1017.58	1016.54	1015.87	1015.23	1015.06	1014.90	1015.05	1015.47
1017.43	1017.72	1017.17	1016.05	1015.25	1014.36	1013.69	1013.61	1013.74	1014.14
1017.49	1017.06	1016.03	1014.82	1014.09	1014.01	1012.63	1012.45	1012.08	1013.24
1020.70	1025.65	1014.90	1013.55	1012.44	1011.97	1011.13	1011.13	1011.50	1012.03
1015.44	1014.12	1012.69	1012.13	1011.46	1011.07	1010.94	1010.71	1010.21	1011.11

Table 4.3 Atmospheric Pressure in Summer 2 (millibars)

1010.90	1010.86	1010.76	1010.54	1010.49	1010.36	1010.75	1010.75	1010.75	1010.55
1011.07	1011.23	1011.56	1011.63	1011.46	1011.10	1011.07	1011.44	1012.14	1011.95
1011.90	1011.90	1012.22	1012.56	1012.73	1012.51	1012.45	1012.59	1012.59	1012.59
1011.79	1012.00	1012.21	1012.84	1012.94	1012.91	1013.07	1012.92	1012.76	1012.37
1011.82	1011.97	1012.24	1012.65	1012.92	1012.91	1013.09	1013.00	1012.77	1012.20
1011.67	1011.92	1012.30	1012.44	1012.89	1012.93	1012.86	1012.74	1012.47	1012.07
1011.47	1012.00	1012.41	1012.73	1012.86	1012.87	1012.66	1012.42	1012.24	1012.02
1011.76	1012.69	1012.70	1012.89	1013.00	1012.78	1012.53	1012.21	1012.07	1011.88
1011.89	1012.44	1013.15	1013.15	1013.00	1012.63	1012.38	1012.11	1012.06	1011.91
1012.32	1013.11	1013.27	1013.08	1012.91	1012.55	1012.35	1012.11	1012.06	1011.90
1012.09	1013.29	1013.35	1013.14	1012.92	1012.58	1012.26	1012.17	1012.07	1011.67
1012.91	1013.20	1013.01	1012.77	1012.64	1012.58	1012.23	1012.13	1011.78	1011.52
1012.65	1012.58	1012.39	1012.27	1012.99	1012.03	1011.87	1012.02	1011.50	1011.17
1012.21	1012.91	1011.79	1011.73	1011.70	1011.71	1011.75	1011.53	1010.75	1010.55

Table 4.4 Atmospheric Pressure in Winter 2 (millibars)

1017.92	1017.46	1017.25	1016.98	1016.49	1016.57	1015.96	1015.85	1015.70	1014.79
1017.40	1017.65	1017.39	1017.18	1017.01	1016.48	1017.40	1017.60	1018.22	1017.46
1016.74	1017.04	1017.61	1017.77	1017.96	1017.90	1017.90	1018.32	1018.51	1018.82
1016.98	1016.92	1017.44	1017.64	1017.60	1017.80	1017.82	1018.34	1018.31	1019.15
1015.17	1015.64	1015.61	1016.29	1016.36	1016.78	1016.78	1017.70	1017.57	1018.52
1014.24	1014.71	1015.18	1015.47	1015.46	1015.17	1014.40	1015.64	1017.41	1018.34
1013.74	1013.90	1014.10	1014.12	1014.14	1013.97	1014.25	1013.60	1015.51	1016.93
1012.98	1013.13	1013.05	1012.95	1012.35	1011.57	1012.46	1012.81	1014.46	1016.11
1012.27	1012.97	1012.85	1011.97	1011.26	1010.40	1011.19	1011.60	1012.74	1014.29
1012.40	1012.94	1013.16	1010.59	1010.13	1009.57	1010.07	1010.39	1011.13	1012.89
1012.49	1012.53	1011.71	1010.53	1009.67	1008.97	1009.07	1009.44	1010.29	1011.88
1012.39	1011.85	1010.88	1009.82	1009.15	1008.51	1008.64	1008.91	1010.27	1011.99
1011.75	1010.76	1009.82	1009.20	1008.64	1008.53	1008.42	1008.61	1009.88	1011.38
1010.67	1009.68	1008.82	1008.43	1008.18	1008.19	1008.27	1008.79	1010.21	1011.54

Table 4.5   Ocean Heights (cms)

34.00	39.00	38.00	37.00	36.00	35.00	45.00	38.00	37.00	38.00	35.00	34.50	34.00
46.00	42.00	44.00	42.00	50.00	38.00	38.00	39.00	38.00	39.00	36.00	34.00	33.00
42.00	39.00	56.00	60.00	31.00	55.00	32.00	40.00	36.00	32.00	31.00	33.00	32.00
42.00	40.00	41.00	60.00	51.00	32.00	46.00	42.00	33.00	30.00	30.00	31.00	30.00
38.00	49.00	41.00	41.00	48.00	46.00	42.00	34.50	33.00	26.00	22.00	32.00	29.00
37.00	43.00	55.00	55.00	46.00	32.00	31.00	30.50	26.00	22.00	19.00	30.00	29.00
38.00	43.00	30.00	32.00	34.50	34.00	30.00	28.00	25.00	20.00	19.00	29.00	26.50
39.00	42.00	46.00	46.00	42.00	34.00	30.00	30.00	25.00	20.00	19.00	26.00	25.00
39.00	43.00	30.00	46.00	36.00	32.00	30.00	26.00	22.00	19.00	18.00	23.00	22.00
39.00	42.00	45.00	40.00	36.00	30.00	28.00	26.00	22.00	19.00	18.00	19.00	18.00
26.00	26.00	26.00	37.00	22.00	18.00	20.00	19.00	18.00	18.00	17.00	18.00	17.00
33.00	24.00	31.00	21.00	26.00	26.00	19.00	19.00	20.00	18.00	16.00	17.00	16.00
36.00	21.00	19.00	18.00	18.00	15.00	14.00	15.00	13.00	15.00	15.00	15.00	15.00
20.00	11.00	12.00	15.00	14.00	13.00	13.00	13.00	13.00	13.00	13.00	13.00	13.00